

Curvature sensor based on In-fiber Mach-Zehnder Interferometer inscribed with femtosecond laser

D. Pallarés-Aldeiturriaga, L. Rodríguez-Cobo, A. Quintela, and J.M. Lopez-Higuera

Abstract—In this work, an In-fiber Mach-Zehnder Interferometer inscribed by femtosecond laser for curvature sensing has been designed and manufactured. Its operating principle consists of a secondary waveguide inscription working as a sensing arm. This waveguide has been manufactured using asymmetric structures with an average refractive index change of 1.1×10^{-2} in its guiding section measured by refracted near-field profilometry. The overall arm/cladding index difference is higher than its core/cladding counterpart, which is a suggested condition for device operation following preliminary simulations. The manufactured Mach-Zehnder Interferometer exhibits a linear response to bending radius which is also dependent on an established bending axis. Sensitivity has been measured up to $9.49 \text{ nm}/\text{m}^{-1}$ for curvature ranges from 0 to 14 m^{-1} . Simulation results using the Beam Propagation Method and conformal mapping transformation to convert bending action into a tilt refractive index agree with experimental results for the same index parameters. Preliminary temperature test shows a remarkable cross sensitivity of $0.0024(3) \text{ m}^{-1}/^\circ\text{C}$ up to 180°C .

Index Terms—Optical fiber interference, Optical fiber devices, Ultrafast optics.

I. INTRODUCTION

MACH-ZEHNDER Interferometers (MZI) are of particular interest due to high sensitivity and simplicity. Different performances and sensing parameters can be achieved depending on configurations and manufacturing processes. Some common examples are based on fiber tapers, Long Period Gratings (LPGs), core mismatch, air-hole collapsing of PCF and MMF segment, among others [1].

Another remarkable technology that can be used on MZI manufacturing are femtosecond lasers. There are several papers reporting in-fiber MZI inscribed using femtosecond technology, however, their underlying principle consists mainly of an air cavity performed by ablation [2], [3]. This cavity may be in contact with the surrounding fiber medium [2] (exhibiting sensitivity to its surrounding index change) or inside the optical fiber [3] (which is a hybrid technique involving fusion

splicing). Index mode differences exhibited by these configurations are remarkably high, allowing making functional devices with a total length under $100 \mu\text{m}$. Unfortunately, they are unable to detect bending direction and the induced ablation may deteriorate the mechanical response of the device, limiting the maximum bending (before breaking the fiber) that can be reached with that sensor. On the contrary, there are very few examples of MZI using induced Refractive Index Change (RIC) to the best of the authors' knowledge. Said phenomenon exhibits a tremendous potential for waveguide and other microphotonic device development. Femtosecond laser induced RIC usually is classified in smooth positive isotropic RIC (Type I) and birefringent RIC (Type II). The first type displays contrast around $\sim 10^{-3}$, while the second exhibits an overall negative RIC that can reach $\sim -2 \times 10^{-2}$ [4], [5]. Positive index contrast higher than Type I can be also achieved with [6] and without [7] a high Pulse Repetition Rate (PRR) in asymmetric structures, thanks to the significant amount of elastic stress deposited in the material.

There have been reports of waveguide inscription in fiber optics, but with an index change of 3.2×10^{-3} [8], having asymmetric structures not fully explored except for X-couplers [9]. This phenomenon is proposed for the development of an In-fiber Mach-Zehnder Interferometer for direction-sensitive curvature measurement based on a secondary waveguide inscribed by femtosecond laser. The increased index contrast of the waveguide will increase the effective mode index difference, making size reduction possible in comparison to previous reported curvature sensors, that usually exhibit lengths higher than 10mm [10], [11]. This new design should improve the curvature range, with ease of implementation, while not requiring complex adaptive optics for cylindrical geometry compensation.

II. SENSOR DESIGN AND SIMULATION

Mach-Zehnder interferometers present a transmission spectra in the shape of a fringe pattern, they are based on the interference of two different optical paths coming from a splitted beam. One path is set as reference and the other acts as the sensing element. When the interferometer is integrated into an optical fiber, splitting is usually understood as the fundamental mode being decoupled to a secondary mode which propagates through a given length L before being coupled back, interfering with the fundamental mode due to an existing Optical Path Difference (OPD). This interference can be represented by the well known equation

This work has been supported by the projects TEC2013-47264-C2-1-R, TEC2016-76021-C2-2-R (AEI/FEDER, UE) financed with FEDER funds, and grant BES-2014-069736 of the Spanish government and by the Parliament of Cantabria postdoc grant.

D. Pallarés-Aldeiturriaga is with the Photonics Engineering Group, University of Cantabria, 39005, Santander (Spain).

L. Rodríguez-Cobo, A. Quintela, and J.M. Lopez-Higuera are with the Photonics Engineering Group, University of Cantabria, 39005, Santander (Spain), the CIBER-bbn, Instituto de Salud Carlos III, 28029, Madrid (Spain) and Instituto de Investigación Sanitaria Valdecilla (IDIVAL), Cantabria, Spain.

$$I = I_1 + I_2 + 2\sqrt{I_1 I_2} \cos\left(\frac{2\pi\Delta n L}{\lambda} + \phi_0\right), \quad (1)$$

where I_1 and I_2 represent fundamental and secondary irradiances respectively, $\Delta n = n_2 - n_1$ is the effective mode index difference between cited modes and L is the path length. The transmission spectrum will present a sinusoidal shape with local minima which is commonly referred to as an *interference dip*. Any disturbance of $OPD = \Delta n L$ will produce a displacement of the dip wavelength $\lambda_{dip} = 2\Delta n L / (2m + 1)$ that may be employed to quantify the designed measurand.

The proposed design is depicted in Fig. 1. In this case, the mode splitting is achieved by inscribing a secondary waveguide into the optical fiber. Such inscription begins at the core and displaces from the fiber axis with an insertion angle $\theta \in [4.3, 8.5]^\circ$ until a certain spacing from the core is achieved. Afterwards, inscription continues parallel to the core and then returns with the same insertion angle. L is the total sensor length and X represents the waveguide spacing from the core. This design allows a single step inscription, which would imply a great reduction on its manufacturing cost.

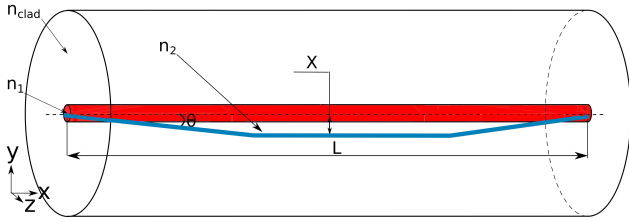


Fig. 1. Depiction of the manufactured geometry. Secondary waveguide begins at the core and displaces to the cladding with a slightly angle θ and then goes back to the core with the same angle.

TABLE I: Simulation Parameters Used in BeamPROP

Parameter	Value
n_{clad}	1.4661
Sensor length (L)	$3000\mu m$
n_1	1.4706
Insertion angle (θ)	4.3°
cladding width	$125\mu m$
Spacing (X)	$30\mu m$
core width	$8\mu m$
secondary core width	$3\mu m$

In order to model fiber bending, a mathematical coordinate transformation called conformal mapping can be employed to transform bending action into a tilt refractive index [12]. This effective index can be represented by the following equation for polar coordinates [13]:

$$n_{bend} = n \left[1 + (r\kappa) \cos(\phi) \right]. \quad (2)$$

Here, $\kappa = 1/R$ is the curvature, the inverse of bending radius R towards bending axis and r, ϕ the polar coordinates as represented in Fig. 2. When bending occurs at the $+Y$ axis direction (for the design depicted in Fig. 1), the effective secondary waveguide mode index decreases, reducing Δn from Eq. 1 and hence, the OPD. Likewise an increment in Δn

(and thus the OPD) occurs when bending takes place in the opposite direction. Based on this dependence phenomenon, a relation between curvature and λ_{dip} can be established, which will be studied by different simulation and experimental tests.

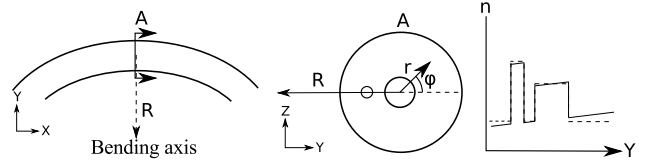


Fig. 2. Model for a bending optical fiber with two cores and its effective index profile due to coordinate transformation.

Several simulations were performed in order to analyse the sensor design using BeamPROP, a commercial software based on the Beam Propagation Method (BPM) [14]. A 2D geometry was considered in order to make simpler and faster calculations. The parameters employed are listed in Table. I, the secondary waveguide refractive index n_2 was set as a free parameter. Results suggest that, for this configuration, n_2 must be higher than n_1 . Interferometric shape is achieved when $\Delta n_2 = n_2 - n_{clad} > 9 \times 10^{-3}$. Bending will be applied to simulated MZI by two methods; the first one is the aforementioned conformal mapping and the second one will simply consist in an actual circle arc bend with Rsoft CAD environment. Both results will be compared and explained in section IV using experimental parameters to correlate with experimental data, suggesting a lineal dependence of Δn with curvature.

III. MANUFACTURING

Based on the simulation results, the index change of the secondary waveguide should be higher than SMF28 core. For that purpose, a waveguide inside a standard SMF28 has been inscribed with a commercial Fiber Laser Chirp Pulse Amplifier (FLCPA) from CALMAR lasers operating at 1030nm, 1.09μJ pulse energy, 370fs pulse duration, focused through an objective lens from Mitutoyo (NA=0.5) at 120kHz repetition rate and 10 μm/s writing speed, resulting in filamentary propagation (depicted in Fig. 3(a)). The produced structure exhibits different refractive index regions in a similar way to Hashimoto *et al* [7]. When the opposing end face is illuminated by a light source, two lightspots are detected: one at the fiber core and another at the filament below the focal volume, at which the laser is focused; this can be noticed in Fig. 3(b). Refracted Near Field profilometry (RNF) [15] by Sira Optical Fibre Refractive index profiler was performed at core and filament as depicted in Fig. 3(c) and Fig. 3(d). Core index change was $\Delta n_1 = 4.50(29) \times 10^{-3}$ while filament had inhomogeneous change varying from 8.9×10^{-3} to 14×10^{-3} with an average value of $\Delta n_2 = 11.00(78) \times 10^{-3}$. This configuration requires focal volume (which has negative refraction index and hence is unable to guide light) to be placed above the core. As the filament is larger than the focal volume, precision requirements in the Z axis are lower than X and Y axes. This waveguide configuration is employed for the proposed design, performing sensor inscription in the same commercial SMF28,

holding the sample over a nanoscale resolution X-Y-Z linear motor stage from Aerotech.

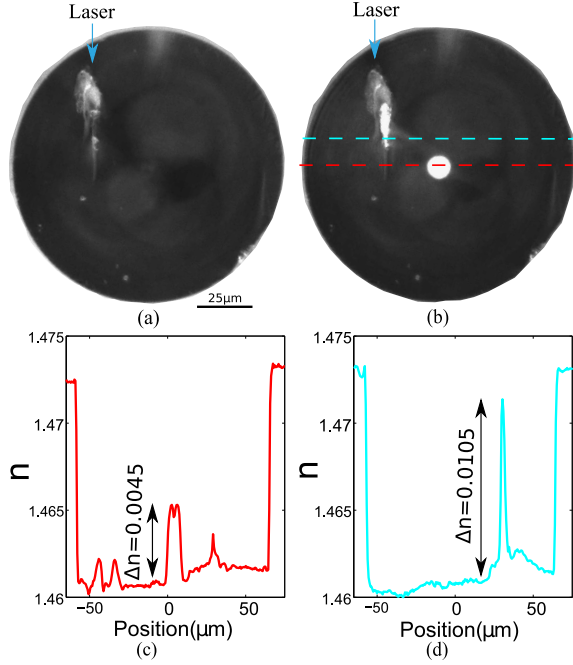


Fig. 3. Inscribed waveguide: CCD transversal capture of the inscription (a), illuminating its opposing end face by a whitelight source (b), core (c) and inscription (d) index profile.

IV. EXPERIMENTAL RESULTS AND DISCUSSION

Several MZI were inscribed with different sensor parameters; some collected spectra are shown in Fig. 4. Typical decrease of Free Spectral Range (FSR) with sensor length L is appreciated at the top of Fig. 4 (spacing $X = 15\mu\text{m}$ and insertion angle $\theta = 8.5^\circ$) while dip sharpness decreases with insertion angle θ as depicted at the bottom of Fig. 4 ($X = 15\mu\text{m}$ and $L = 3\text{mm}$). For $\theta = 1.7^\circ$, the spectrum was irregular due to undesirable mode coupling caused by core/waveguide proximity over a long distance. This effect turns a higher value of X into a requisite to avoid mode coupling interaction while inscription is being performed.

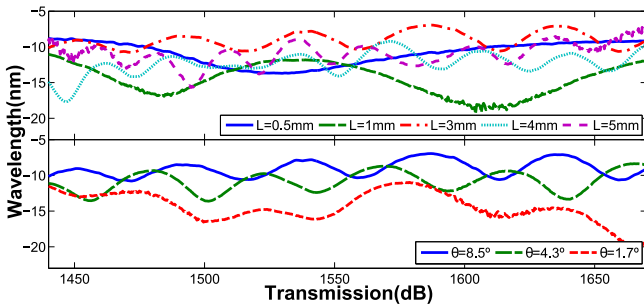


Fig. 4. MZI spectra for parameter comparison: Interferometer length L from 0.5mm to 5mm at $X=15\mu\text{m}$ $\theta = 8.5^\circ$ and insertion angle θ from 1.7° to 8.5° at $X=15\mu\text{m}$ & $L=3\text{mm}$.

In order to measure the applied curvature, the fiber has been clamped on two xyz platforms separated an initial distance

L_f , leaving the sensor in the middle of them as described in Fig. 5(a). One platform remains fixed while the other one is displaced in the X direction. Fiber bending is thus achieved by moving the depicted movable platform in the X axis. Curvature estimation has been achieved using the circumference relation $L_f - x = L_f \text{sinc}\left(\frac{L_f \kappa}{2}\right)$ [11].

Bending direction is also controlled by placing plane YX of the sample perpendicular to the plane YX of design and sandwiching the sensor between two slides, restricting the movements of the sensor and constraining bending to the Y axis only ($+Y$ and $-Y$ (as in Fig. 5(a)) direction).

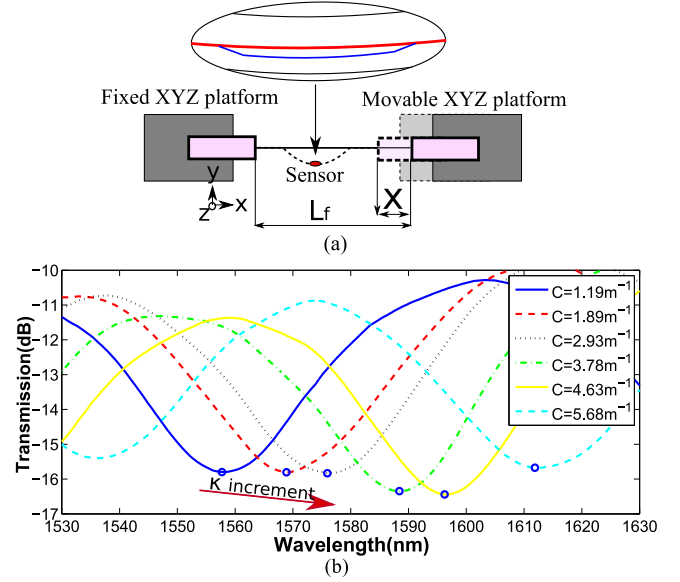


Fig. 5. Curvature measurement scheme (a), MZI spectra for different curvatures ranging from 1.19m^{-1} to 5.68m^{-1} towards $-Y$ direction. Sensor parameters: $L=3\text{mm}$ $\theta = 4.3^\circ$ & $X=30\mu\text{m}$ (b).

When the sensor is bent, the interference dip wavelength λ_{dip} suffers an increment/decrement with respect to bending direction. Bending towards the $-Y$ direction produces an λ_{dip} increment as depicted in Fig. 5 and decreases when bending is produced at the opposite direction. In addition, dip wavelength remains insensitive to Z direction bending. After several measurements with different parameters maximizing X and decreasing θ best sensitivities have been obtained for $\theta = 4.3^\circ$ and $X=30\mu\text{m}$ with a minimum sensor length $L=3\text{mm}$. Sensors with lower L exhibit a sensitivity drop caused by having a relative large coupling zone. Measurements for mentioned parameters are depicted in Fig. 6(a). Experimental data exhibit an approximately linear behaviour with $R^2 = 0.9934$ and $R^2 = 0.9871$ for $+Y$ and $-Y$ directions respectively. Their lineal slopes are $-0.1329(41)(\text{nm} \cdot \text{m})^{-1}$ and $0.1054(64)(\text{nm} \cdot \text{m})^{-1}$, which correspond to a sensitivity of $7.52(23)\text{nm}/\text{m}^{-1}$ and $9.49(58)\text{nm}/\text{m}^{-1}$ for $+Y$ and $-Y$ bending respectively exhibiting a repeatability of 3.45%, obtained by measuring sensitivity 5 times in each direction and selecting the highest deviation from the first measurement. Other bending axis show different responses, improving their sensitivity with the alignment to Y axis. This dependency is deduced from Eq. (2), where maximum index increment/decrement occurs when

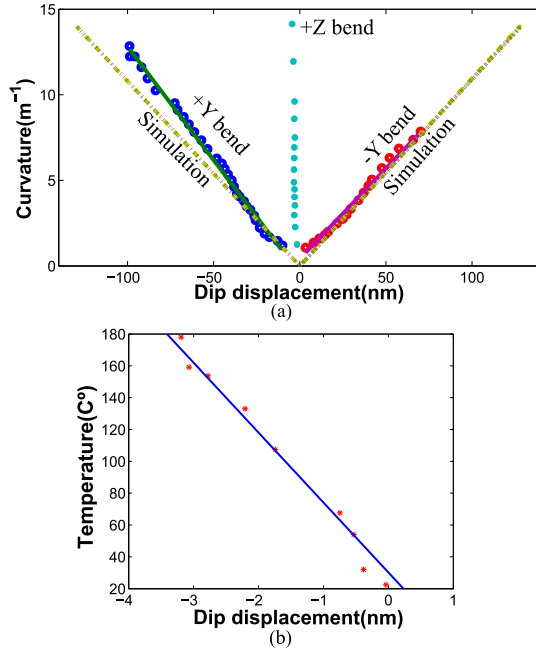


Fig. 6. (a) Experimental measures of the dip wavelength displacement with curvature for the three given bending axes (+Y, -Y, +Z) and the simulation results for both conformal mapping and actual bend for the horizontal axes (+Y, -Y); (b) Experimental variation of the dip wavelength displacement with temperature.

parallel to that axis bending whereas perpendicular bending produces no overall OPD.

Simulations are also depicted in Fig. 6(a) for the same parameters and measured index difference in previous section. Both conformal mapping and circular bending simulations are in good agreement with each other having λ_{dip} lineal and symmetric dependency with curvature. Experimental data differ 23%(+Y) and 3.8%(-Y) from them. This slightly asymmetry in +Y may be explained as a consequence of waveguide inhomogeneities in refractive index and cross-section caused by stress forces located inside the filament. Irregular cross-section and refractive index could induce different modal effective index dependences with curvature with respect to the bending plane. Several simulations introducing sinusoidal perturbations in longitudinal and transversal profiles have been performed, while symmetry and linear dependence have remained unaltered. In addition, the compression or stretching associated with the bending might be perturbed by the inscription itself as it is a source of permanent strain and elastic stress that could induce a certain deviation from Eq. 2. This in turn, could alter λ_{dip} response with bending axis direction.

A temperature study has been also performed to analyse the effect of cross-sensitivity in the sensor. This dependency is depicted in Fig. 6(b) where an approximately linear tendency is appreciated in the range 25-180 $^{\circ}C$ where the sensitivity was found to be 0.0228(22)nm/ $^{\circ}C$. The sensor cross sensitivity is therefore as low as 0.0024(3) $m^{-1}/^{\circ}C$.

V. CONCLUSION

A compact curvature sensor based on an In Fiber MZI

inscribed by femtosecond laser has been presented and experimentally verified. Manufactured waveguides employed in its operating principle exhibit an average index change of 1.1×10^{-2} being single step inscription without requiring high precision inscription (especially in Z axis) nor adaptive optics. Sensor response is linear in a remarkable broad curvature range from 0 to 14 m^{-1} and achieving sensitivities up to 9.49nm/ m^{-1} . Results are in good agreement with performed simulations using parameters obtained in waveguide characterization process. Sensitivity dependence to bending axis has been shown, being the axis parallel to core/waveguide the best result in terms of sensitivity while perpendicular bending shows an insensitive response. Slight asymmetries have been detected when inverting the bending axis direction. The inhomogeneous waveguide cross section and stress deposition can be one of the causes of the detected asymmetry. Other waveguide inscription methods and designs should be performed in order to improve sensitivity and control its dependence with the bending axis.

ACKNOWLEDGMENT

The authors would like to thank Arturo Pardo Franco for his careful manuscript revision.

REFERENCES

- [1] B. H. Lee, Y. H. Kim, K. S. Park, J. B. Eom, M. J. Kim, B. S. Rho, and H. Y. Choi, "Interferometric fiber optic sensors," *Sensors* **12**, 2467-2486 (2012).
- [2] M. Dębowska, Anna K. and Koba, Marcin and Janik, Monika and Bock, Wojtek J. and Śmietana, "Increased sensitivity of femtosecond laser micro-machined in-fiber Mach-Zehnder interferometer for small-scale refractive index sensing," *Proc. SPIE* **9916**, 99160Q-99160Q-4 (2016).
- [3] H. Gong, D. N. Wang, B. Xu, K. Ni, H. Liu, and C. L. Zhao, "Optical fiber internal mirror based fiber in-line Mach-Zehnder interferometer," *Proc. SPIE* **9916**, 99161U-99161U-4 (2016).
- [4] M. Desmarchelier, R. Poumellec, B., Brisset, F., Mazerat, S. and Lancry, "In the Heart of Femtosecond Laser Induced Nanogratings : From Porous Nanoplanes to Form Birefringence Development of Nanostructure Formation of State on Heat Treatment," *World Journal of Nano Science and Engineering* **5**, 115-125 (2015).
- [5] K. Mishchik, C. D'Amico, P. K. Velpula, C. Maclair, A. Boukenter, Y. Ouerdane, and R. Stoian, "Ultrafast laser induced electronic and structural modifications in bulk fused silica," *Journal of Applied Physics* **114** (2013).
- [6] S. M. Eaton, M. L. Ng, R. Osellame, and P. R. Herman, "High refractive index contrast in fused silica waveguides by tightly focused, high-repetition rate femtosecond laser," *Journal of Non-Crystalline Solids* **357**, 2387-2391 (2011).
- [7] F. Hashimoto, T. Yoshino, Y. Ozeki, and K. Itoh, "Large increase in refractive index inside silica glass after the movement of voids caused by femtosecond laser pulses," *Japanese Journal of Applied Physics* **042601** (2014).
- [8] C. Waltermann, A. Doering, M. Köhring, M. Angelmahr, and W. Schade, "Cladding waveguide gratings in standard single-mode fiber for 3D shape sensing," *Optics Letters* **40**, 3109 (2015).
- [9] C. Lin, C. Liao, J. Wang, J. He, Y. Wang, Z. Li, T. Yang, F. Zhu, K. Yang, Z. Zhang, and Y. Wang, "Fiber surface Bragg grating waveguide for refractive index measurements," *Optics Letters* **42**, 1684 (2017).
- [10] T. Allsop, K. Kalli, K. Zhou, Y. Lai, G. Smith, M. Dubov, D. J. Webb, and I. Bennion, "Long period gratings written into a photonic crystal fibre by a femtosecond laser as directional bend sensors," *Optics Communications* **281**, 5092-5096 (2008).
- [11] S. Zhang, W. Zhang, S. Gao, P. Geng, and X. Xue, "Fiber-optic bending vector sensor based on Mach-Zehnder interferometer exploiting lateral-offset and up-taper," *Optics Letters* **37**, 4480 (2012).
- [12] C. Schulze, A. Lorenz, D. Flamm, A. Hartung, S. Schröter, H. Bartelt, and M. Duparré, "Mode resolved bend loss in few-mode optical fibers," *Optics Express* **21**, 3170 (2013).

- [13] D. Marcuse, "Field deformation and loss caused by curvature of optical fibers," *America* (1976).
- [14] R. Scarmozzino, A. Gopinath, R. Pregla, and S. Helfert, "Numerical techniques for modeling guided-wave photonic devices," *IEEE Journal on Selected Topics in Quantum Electronics* **6**, 150-162 (2000).
- [15] K. I. White, "Practical application of the refracted near-field technique for the measurement of optical fibre refractive index profiles," *Optical and Quantum Electronics* **11**, 185-196 (1979).